

Publication P1

Sami Ruoho, Emad Dlala, and Antero Arkkio. 2007. Comparison of demagnetization models for finite-element analysis of permanent-magnet synchronous machines. IEEE Transactions on Magnetics, volume 43, number 11, pages 3964-3968.

© 2007 Institute of Electrical and Electronics Engineers (IEEE)

Reprinted, with permission, from IEEE.

This material is posted here with permission of the IEEE. Such permission of the IEEE does not in any way imply IEEE endorsement of any of Aalto University's products or services. Internal or personal use of this material is permitted. However, permission to reprint/republish this material for advertising or promotional purposes or for creating new collective works for resale or redistribution must be obtained from the IEEE by writing to pubs-permissions@ieee.org.

By choosing to view this document, you agree to all provisions of the copyright laws protecting it.

Comparison of Demagnetization Models for Finite-Element Analysis of Permanent-Magnet Synchronous Machines

Sami Ruoho^{1,2}, Emad Dlala¹, and Antero Arkkio¹

¹Laboratory of Electromechanics, Helsinki University of Technology, FIN-02015 TKK, Finland

²Neorem Magnets Oy, FIN-28400 Ulvila, Finland

We have studied a few simple demagnetization models, which are quick and easy to implement in finite-element calculations, and compared them with measured recoil behavior of Nd–Fe–B magnet material, also using a hysteresis model for comparison. The models are used to estimate post-demagnetization performance of an overloaded surface magnet synchronous machine. Two of the simple models, the sloped linear model and the exponent function model, give the most accurate results without significantly increasing the computation time.

Index Terms—Demagnetization, finite-element analysis, magnetic field modeling, permanent magnets, synchronous machines.

I. INTRODUCTION

PERMANENT-MAGNET machines are designed to remain undemagnetized in normal working conditions. In some cases, like when the machine is overloaded or after a short circuit, the machine performance can be degraded due to partial permanent-magnet demagnetization. A suitable model is needed to evaluate the machine performance after the demagnetization.

In this paper, several simple demagnetization models are studied. Some of these models can be used to help a designer detect demagnetization risks. More accurate models can be used to simulate real behavior during and after the demagnetization. A hysteresis model is used for comparison.

The focus here is on modeling permanent magnets using two-dimensional time-stepping finite-element analysis. A more complete description of the methods used in the finite-element solution of the magnetic field with circuit equations for the whole machine is available in [1].

For simple demagnetization models, the system of equations is solved using the Newton–Raphson iteration method. For the hysteresis model, the fixed-point method iteration must be used to guarantee convergence. The fixed-point technique is stable and thus will be used for solving the hysteretic problem.

The permanent magnet is characterized only for its two distinct directions, the easy axis and the hard axis. Since the focus of this paper is on modeling permanent magnet, the nonlinearity of the rotor and stator cores is modeled using a single-valued magnetization curve.

Simple models have been earlier used by Kang *et al.* [2], [3], Lee *et al.* [4] and Kim *et al.* [5]. They have described models which are referred as linear models in this paper. The method of their calculations is clearly described in the paper of Lee *et al.* [4]. Farooq *et al.* [6] have used a permeance network model to simulate the performance of demagnetized motor. However, their model does not include demagnetization within the calculations.

II. RECOIL BEHAVIOR OF Nd–Fe–B MAGNET MATERIAL

In this work, three different Nd–Fe–B magnet grades were measured to get representing recoil curves. The measurements

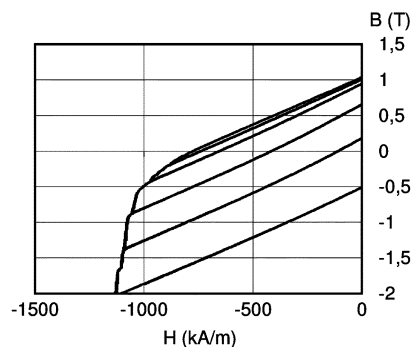


Fig. 1. Recoil curves of a high coercivity Nd–Fe–B magnet grade at 120 °C. The measurement was performed using manually controlled hysteresis-graph. The set of curves here is a result of a single measurement of a single $10 \times 10 \times 10$ mm³ sample. A commercial magnet grade was used.

were performed in three different temperatures, which all were close to the normal electric machine working temperatures. Fig. 1 shows five recoil curves of a high coercivity magnet grade at 120 °C.

The measurements lead to the following conclusions. For Nd–Fe–B magnet, the recoil line is almost a straight line, especially, with small demagnetization. With larger demagnetization, the recoil line is slightly but clearly bent upwards near *B*-axis. An important matter to be noticed is that the recoil curve does not form a significant minor loop if *B*-axis is not crossed. However, if *B*-axis is crossed during the recoil operation, a clear minor loop is formed. In that case, the minor loop is not symmetric (Fig. 2).

A. Temperature Dependence of Magnetic Properties

The temperature dependencies of remanence and intrinsic coercivity are usually treated with temperature coefficients for Nd–Fe–B magnets. This leads to first-order relations between the mentioned properties and temperature. However, the remanence of a ferromagnetic material as a function of temperature does not form a straight line at least within the whole temperature range below Curie temperature [7]. To cope with this nonlinearity, some manufacturers give different temperature coefficients for different temperature ranges.

In this work, the remanence of one Nd–Fe–B-sample was measured at six different temperatures between the room temperature and 120 °C (Fig. 3). Both first-order and second-order polynomials were fitted to the data.

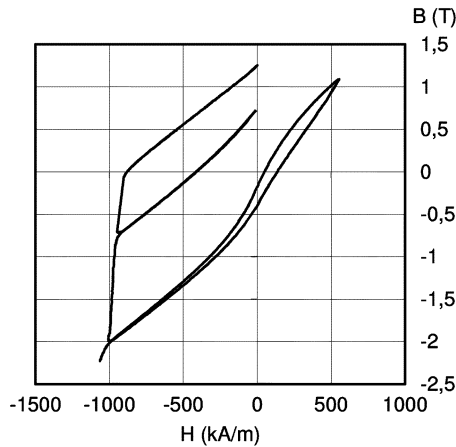


Fig. 2. A recoil curve and a minor loop of a Nd–Fe–B-magnet sample. Note, that a significant minor loop is formed only, when the B -axis is crossed during recoil operation.

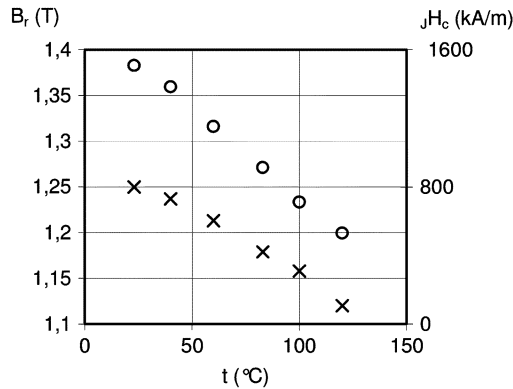


Fig. 3. Remanence (crosses) and intrinsic coercivity (circles) of Nd–Fe–B-sample as a function of temperature.

The average difference between all the measured data points and fitted first-order polynomial was 0.4%. The average difference between the measured data and fitted second-order polynomial was 0.2%.

From these results, it can be concluded that the first-order approximation for temperature dependence of remanence can be used for the whole measured temperature range. From previous measurements, it is known that somewhat linear temperature behavior can be also expected at higher temperatures, but below 200 °C.

The intrinsic coercivity of the same sample was also measured at the same temperatures (Fig. 3). The results clearly show a linear temperature dependence of the intrinsic coercivity.

III. SIMPLE DEMAGNETIZATION MODELS

In this section, different simple demagnetization models and the iteration scheme used are described. In all simple models, the B – H -behavior is described along the easy axis only. The hard axis is assumed to be linear.

A. Method of Calculation

All these simple models can be defined with only a few parameters: remanence, intrinsic coercivity, slope (recoil permeability), and a curve shape parameter (for some models only). The remanence and intrinsic coercivity are defined in two different temperatures. The actual values at working temperature are calculated by linear interpolation.

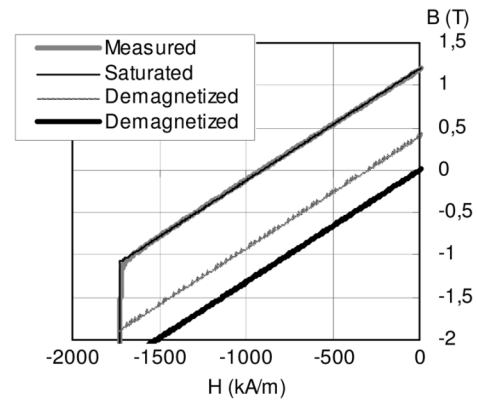


Fig. 4. B – H -behavior of linear sloped model compared to a measured curve. In linear vertical model, the steeply falling part of B – H -curve would be exactly vertical causing some difference to the measured data.

Crank–Nicholson time-stepping FEM analysis using Newton–Raphson iteration [1] is used for these demagnetization calculations. The flux density at each time step is first calculated using a linear model for the magnet material, where only remanence and slope are defined. After the solution has converged, a working point for each element with permanent-magnet material is checked.

If the working point is too far on the negative H -axis when compared to the curve given by the demagnetization model, the remanence of that element is reduced to bring the working point back to the B – H -curve. If there have been changes in the remanences during these checks, the flux density at the time step will be recalculated using the updated remanence values and checked again.

B. Limit Model

In this model, three parameters are needed: remanence, slope and intrinsic coercivity. The intrinsic coercivity jH_c is given as a limiting value. If the working point in an element is below jH_c , the magnetization in that element is changed to be zero.

C. Linear Models

There are two linear models, which are referred to as “linear vertical” and “linear sloped” models.

In the linear vertical model, three parameters are needed: remanence, slope, and intrinsic coercivity. The intrinsic coercivity jH_c is given as a limiting value. If the working point in an element is below jH_c , the magnetization in that element is changed according to the working point and recoil permeability.

In the linear sloped model, four parameters are needed: remanence, slope of recoil line, intrinsic coercivity, and slope of coercivity limit. If the working point in an element is beyond the almost vertical coercivity limit line, the magnetization in that element is changed according to the working point and recoil permeability (Fig. 4).

D. Exponent Function Model

In the exponent function model, the B – H -behavior is described with four parameters: remanence, slope of recoil line, intrinsic coercivity and an additional parameter K_1 describing the sharpness of the knee in B – H -curve (Fig. 5). With larger K_1 -values, the knee in B – H -curve is sharper and vice versa.

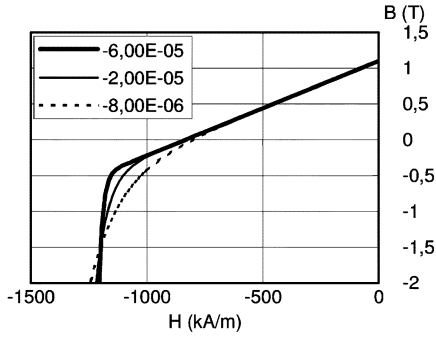


Fig. 5. Effect of parameter K_1 on the curvature of the exponent function model. With value $K_1 = -6 \cdot 10^{-5}$ calculated curve follows accurately the measured curve.

By adjusting this parameter, a good agreement with measured data can be achieved.

The B - H -curve is described with the following function:

$$B = B_r + \mu_0 \mu_r \cdot H - E \cdot e^{K_1} \cdot (K_2 + H) \quad (1)$$

where E is a constant needed for unit conversion. $E = 1$ T. Parameter K_2 is calculated with the following equation:

$$K_2 = \frac{\ln \left[(B_r + (\mu_r - 1) \cdot \mu_0 \cdot J H_c) \cdot \frac{1}{E} \right]}{K_1} - J H_c. \quad (2)$$

With this model, a good agreement with the measured hysteresis curves and calculated B - H -curves can be achieved if K_1 has a value around $-6 \cdot 10^{-5}$ mA.

IV. HYSTERESIS MODEL

The magnetization behavior of permanent magnets is generally similar to soft magnetic materials but yet permanent magnets exhibit wide hysteresis loops the modeling of which by conventional (history-independent) hysteresis models [8]–[10] requires extra treatment. Although the Preisach model has been commonly used for modeling magnetic materials including permanent magnets [11], [12], the model can considerably suffer from the congruency problem [13]. The inverted Preisach model [14] is usually a better choice; however, the model can also be vulnerable to the specific B congruency in some regions of the loop.

A. History-Dependent Hysteresis Model

Obtaining accurate and general physical modeling of hysteresis requires the development of models that take the H congruency along with the B congruency into account. The search of the curve to be modeled has to be carried out over the whole B - H -plane, not only in the horizontal direction (or in the vertical direction). A non-Preisach (equation-free) model of such competence is proposed by Zirka *et al.* [13]. The model is based on constructing the particular segment to be modeled from first-order reversal curves, and the model stores previous reversals and is hence called a history-dependent (HD) hysteresis model. The modeled curve is constructed by interpolating between the first-order reversal curves, and thus it is assumed that an infinite number of first-order reversal curves can be generated by interpolation. The search of the desired curve is needed only at the reversals and it is done using an efficient technique.

The HD hysteresis model is exceptionally accurate and also convenient to be used for the finite-element analysis because it

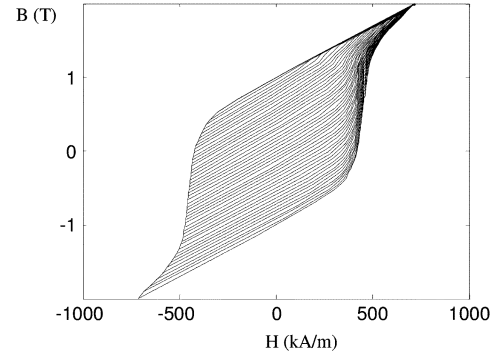


Fig. 6. A set of first-order reversal curves calculated with the used model.

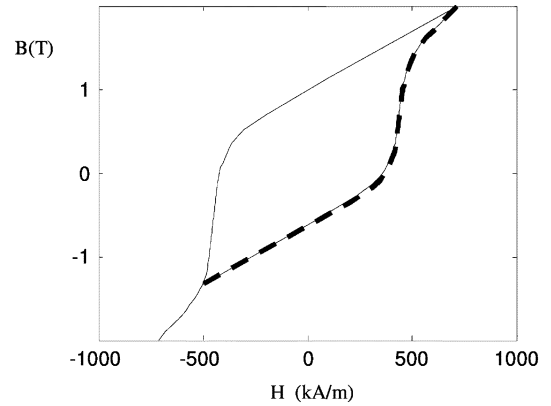


Fig. 7. Comparison of calculated (dashed) and measured (solid) B - H -reversal curves. It can be seen that the curves are almost the same.

does not need inversion and it can be naturally applied in two fashions as $H(B)$ or $B(H)$.

In Fig. 6, a family of first-order reversal curves is created from the major loop using a transplantation method similar, in principle, to Zirka's approach [15]. The method is based on splitting the major loop into three parts where each part uses a specific weighting function that can be identified from measurement, if available. In our case, because a few first-order reversal curves in addition to the major loop were experimentally obtained, the weighting functions have been identified from measurement. The constructed first-order reversal curves have been tabulated for the HD hysteresis model. The accuracy of the model has been evaluated by comparing the measured and modeled data as shown in Fig. 7. Because the HD hysteresis model is capable of reproducing the first-order reversal curves exactly [13], accurate curves will be achieved for the entire set of Fig. 6.

B. Method of Analysis

The fixed-point method formulates the nonlinear magnetic problem in the following manner:

$$\mathbf{R} = \mathbf{H} - \nu_{FP} \mathbf{B} \quad (3)$$

where \mathbf{R} is a magnetization-like quantity to be computed iteratively. The fixed-point coefficient ν_{FP} is a reluctivity-like quantity, which must be constant during iteration and should be properly chosen to ensure contraction.

The hysteresis model is used in the easy axis, m , while the hard axis, d , is assumed to have linear characteristics. Thus, only the relation $H_m = F(B_m)$ is handled by the HD hysteresis

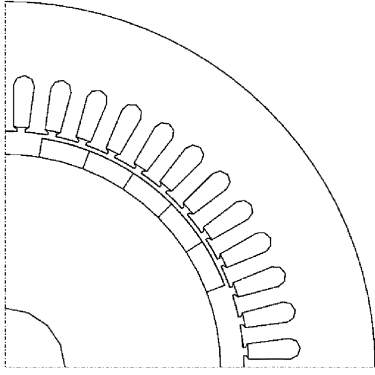


Fig. 8. Example machine used in these simulations.

model and the linear relation $H_d = \nu_0 B_d$ is applied in the hard axis. The flux density components of the easy and hard axes are computed as

$$\begin{aligned} B_m &= B_x \cos \alpha_m + B_y \sin \alpha_m \\ B_d &= B_x \cos \alpha_m - B_y \sin \alpha_m \end{aligned} \quad (4)$$

and subsequently the magnetic field strength in the x and y directions are

$$\begin{aligned} H_x &= H_m \cos \alpha_m + H_d \sin \alpha_m \\ H_y &= H_m \sin \alpha_m - H_d \cos \alpha_m \end{aligned} \quad (5)$$

where α_m is the angle of magnetization.

The fastest convergence of the fixed-point method according to [16] occurs when the fixed-point coefficient ν_{FP} is chosen at time-step n as

$$\nu_{FP}^{(n)} = \frac{C}{2} \left[\frac{\partial H_x^{(n-1)}}{\partial B_x} + \frac{\partial H_y^{(n-1)}}{\partial B_y} \right], \quad \text{for } C > 1 \quad (6)$$

C is a constant and must be conveniently chosen to ensure fast convergence.

Employing the magnetic vector potential \mathbf{A} as an unknown variable, and considering eddy currents in the permanent magnet with conductivity σ , we obtain

$$\nabla \times \nu_{FP} (\nabla \times \mathbf{A}) + \sigma \frac{\partial \mathbf{A}}{\partial t} = -\nabla \times \mathbf{R}. \quad (7)$$

This equation is discretized using finite-element method and solved by the Crank–Nicholson time-stepping scheme.

V. CALCULATIONS WITH AN EXAMPLE MACHINE

There are two purposes for these calculations: To see how the modeling of demagnetization affects the computation time, and to compare different demagnetization models.

A. Example Machine

A virtual surface magnet machine was used in these simulations. The machine is shown in Fig. 8. The main properties of the machine are given in Table I.

One quarter of the machine was modeled. First-order elements were used for the FEM analysis. The finite-element mesh of the machine contained 1142 elements and 779 nodes. The magnets were modeled using 245 elements and 159 nodes.

TABLE I
MAIN PARAMETERS OF THE MODELED MACHINE

Parameter:	Value
Number of Poles	4
Outer diameter of the stator	310 mm
Air gap diameter	200 mm
Core length	246 mm
Number of stator slots	48
Connection	Star
Input Frequency	50 Hz
Rated Voltage	400 V
Rated Power	40 kW
Remanence of PM material in 20°C	1.2 T
Intrinsic coercivity of PM material in 20°C	-1750 kA/m
Remanence of PM material in 150°C	1.0 T
Intrinsic coercivity of PM material in 150°C	-440 kA/m

TABLE II
CALCULATION RESULTS

Iteration Method	Demagnetization Model	Change in EMF	Calculation Time (s)
Newton-Raphson	No demag.	0 %	35
Newton-Raphson	Limit model	-34 %	35
Newton-Raphson	Linear vertical	-13 %	39
Newton-Raphson	Linear sloped	-15 %	38
Newton-Raphson	Exponent	-15 %	39
Fixed point	No demag.	0 %	40
Fixed point	Hysteresis	-7 %	41

B. Test Condition

The simulations were done assuming that the motor is overheated. The rotor temperature and thus the temperature in the PM material were assumed to be 150 °C. The loading was 580 Nm, which is more than twice the rated torque.

First, the no-load voltage was calculated. Then, the machine was run at a constant speed for two periods using a demagnetization model or a hysteresis model. After that the no-load voltage was calculated again. The simulation times were also recorded.

C. Results

The results of different calculations can be seen in Table II. The first two columns show the iteration method and demagnetization model used. The no-load voltage at 150 °C was 355 V. The column “Change in EMF” shows a relative drop in the no-load voltage caused by partial demagnetization when overloading the overheated machine. The last column shows the time needed to simulate the two periods. One period was divided into 400 time steps.

D. Discussions

It can be seen that there are no significant differences in the calculation times between the used iteration methods or demagnetization models. This is because only one-fifth of all the nodes were within magnets, where the demagnetization models were utilized. Thus, the demagnetization calculations can be included in the normal FEM calculations without significant changes in the calculation performance.

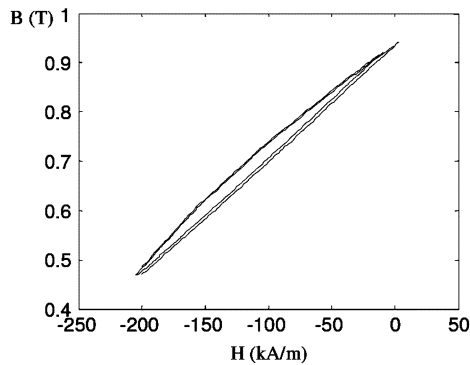


Fig. 9. Working point changes in a point of permanent magnet in the example machine during the simulation when using hysteresis model (note the minor loop.)

The simple limit model gives a too large demagnetization. However, because this model is easy to implement, it can be used to give guidelines in machine design since machines are designed to remain undemagnetized.

Linear vertical model is easy to implement but gave slightly optimistic results on the demagnetization performance. However, because this model does not require any extra parameters (only the basic material properties of permanent magnet must be known), it is easy to use in machine design. The exponent model and linear sloped model both give the same results. This is because the B - H -curve shape parameter was fitted according to the measured data. These models are assumed to give most correct results of all the models tested here because they model quite well the real measured recoil curves (Fig. 1). These two models can be used to simulate the post-demagnetization performance.

The B - H -curve could also be modeled with some other function than the exponent function. Within this research, a polynomial based model and a rational polynomial based model were also tested. With polynomial model, very high-order exponents must be used to force the polynomial curve to follow the measured data. These high-order exponents can lead to numerical problems. The singularities of rational polynomials may also lead to numerical problems.

The hysteresis model used here gave optimistic performance values after demagnetization. This is because the model creates minor loops (Fig. 9), which does not happen in this extent in the real recoil operation of Nd-Fe-B magnet (Fig. 1). A hysteresis model would, however, be useful to estimate both the magnetization and demagnetization performance of Nd-Fe-B magnets in electrical machines. However, this model would need some more development to describe the Nd-Fe-B magnet behavior accurately.

VI. CONCLUSION

A comparison of a set of different simple demagnetization models and a hysteresis model used in 2-D FEM analysis of an electrical machine was presented. The measured recoil behavior of Nd-Fe-B magnet material was also described. The simple models with constant slope recoil curve described better the real behavior of Nd-Fe-B material than the hysteresis model used

here, because the hysteresis model formed minor loops with significant loop area. These kinds of loops were not observed in the measurements. The use of demagnetization models increased the computation times only slightly.

ACKNOWLEDGMENT

This work was supported in part by Finnish Cultural Foundation, Fortum Foundation and Academy of Finland. S. Ruoho would like to thank Dr. Masato Sagawa for discussion concerning Nd-Fe-B-magnet recoil behavior.

REFERENCES

- [1] A. Arkkio, "Analysis of induction motors based on the numerical solution of the magnetic field and circuit equations," Ph.D. thesis, Acta Polytechnica Scandinavica, no. 59, 1987.
- [2] G.-H. Kang, J. Hur, H.-G. Sung, and J.-P. Hong, "Optimal design of spoke type BLDC motor considering irreversible demagnetization of permanent magnet," in *Proc. 6th Int. Conf. Electr. Machines Syst.*, Beijing, China, 2003, vol. 1, pp. 234–237.
- [3] G.-H. Kang, J. Hur, H. Nam, J.-P. Hong, and G.-T. Kin, "Analysis of irreversible magnet demagnetization in line-start motors based on the finite-element method," *IEEE Trans. Magn.*, vol. 39, no. 3, pp. 1488–1491, May 2003.
- [4] B.-K. Lee, G.-H. Kang, J. Hur, and D.-W. You, "Design of spoke type BLDC motors with high power density for traction applications," in *Conf. Rec. 2004 IEEE Ind. Appl. Conf. 39th IAS Annu. Meeting*, Seattle, WA, 2004, vol. 2, pp. 1068–1074.
- [5] K.-C. Kim, S.-B. Lim, D.-H. Koo, and J. Lee, "The shape design of permanent magnet for permanent magnet synchronous motor considering partial demagnetization," *IEEE Trans. Magn.*, vol. 42, no. 10, pp. 3485–3487, Oct. 2006.
- [6] J. Farooq, S. Srairi, A. Djerdir, and A. Miraoui, "Use of permeance network method in the demagnetization phenomenon modeling in a permanent magnet motor," *IEEE Trans. Magn.*, vol. 42, no. 4, pp. 1295–1298, Apr. 2006.
- [7] D. Jiles, *Introduction to Magnetism and Magnetic Materials*. London, U.K.: Chapman & Hall, 1991, p. 191.
- [8] J. Saitz, "Magnetic field analysis of electric machines taking ferromagnetic hysteresis into account," Ph.D. thesis, Acta Polytechnica Scandinavica, no. 107, p. 123, 2001.
- [9] I. D. Mayergoyz, *Mathematical Models of Hysteresis*. New York: Springer-Verlag, 1991.
- [10] D. C. Jiles and D. L. Atherton, "Theory of ferromagnetic hysteresis," *J. Appl. Phys.*, vol. 55, pp. 2115–2120, 1984.
- [11] M. Rosu, J. Saitz, and A. Arkkio, "Hysteresis model for finite-element analysis of permanent-magnet demagnetization in a large synchronous motor under a fault condition," *IEEE Trans. Magn.*, vol. 41, no. 6, pp. 2118–2123, Jun. 2005.
- [12] D. Xie, W. Zhang, B. Bai, and L. Zeng, "Finite element analysis of permanent magnet assembly with high field strength using Preisach theory," *IEEE Trans. Magn.*, vol. 43, no. 4, pp. 1393–1396, Apr. 2007.
- [13] S. E. Zirka, Y. Moroz, P. Marketos, and A. J. Moses, "Congruency-based hysteresis models for transient simulation," *IEEE Trans. Magn.*, vol. 40, no. 2, pp. 390–399, Mar. 2004.
- [14] E. Dlala, J. Saitz, and A. Arkkio, "Inverted and forward preisach models for numerical analysis of electromagnetic field problems," *IEEE Trans. Magn.*, vol. 42, no. 8, pp. 1963–1973, Aug. 2006.
- [15] S. E. Zirka and Y. Moroz, "Hysteresis modeling based on similarity," *IEEE Trans. Magn.*, vol. 35, no. 4, pp. 2090–2096, Jul. 1999.
- [16] E. Dlala, A. Belahcen, and A. Arkkio, "Locally convergent fixed-point method for solving time-stepping nonlinear field problems," *IEEE Trans. Magn.*, vol. 43, no. 11, pp. 3969–3975, Nov. 2007.